Spatial Ca^{2+} Distribution in Contracting Skeletal and Cardiac Muscle Cells

M. E. Zoghbi,* P. Bolaños,* C. Villalba-Galea,*‡ A. Marcano,‡ E. Hernández,‡ M. Fill,† and A. L. Escobar*‡
Instituto Venezolano de Investigaciones Científicas, *Centro de Biofísica y Bioquímica, ‡Centro de Física, Pipe, Venezuela, and †Department of Physiology, Loyola University of Chicago, Maywood, Illinois 60153 USA

ABSTRACT The spatiotemporal distribution of intracellular Ca^{2+} release in contracting skeletal and cardiac muscle cells was defined using a snapshot imaging technique. Calcium imaging was performed on intact skeletal and cardiac muscle cells during contractions induced by an action potential (AP). The sarcomere length of the skeletal and cardiac cells was ~2 μm. Imaging Rhod-2 fluorescence only during a very brief (7 ns) snapshot of excitation light minimized potential image-blurring artifacts due to movement and/or diffusion. In skeletal muscle cells, the AP triggered a large fast Ca^{2+} transient that peaked in less than 3 ms. Distinct subsarcomeric Ca^{2+} gradients were evident during the first 4 ms of the skeletal Ca^{2+} transient. In cardiac muscle, the AP-triggered Ca^{2+} transient was much slower and peaked in ~100 ms. In contrast to the skeletal case, there were no detectable subsarcomeric Ca^{2+} gradients during the cardiac Ca^{2+} transient. Theoretical simulations suggest that the subsarcomeric Ca^{2+} gradients seen in skeletal muscle were detectable because of the high speed and synchrony of local Ca^{2+} release. Slower asynchronous recruitment of local Ca^{2+} release units may account for the absence of detectable subsarcomeric Ca^{2+} gradients in cardiac muscle. The speed and synchrony of local Ca^{2+} gradients are quite different in AP-activated contracting cardiac and skeletal muscle cells at normal resting sarcomere lengths.

INTRODUCTION

In skeletal and cardiac muscle, depolarization of the transverse tubular (T-tube) membrane by the action potential (AP) triggers Ca^{2+} release from the sarcoplasmic reticulum (SR), an intracellular Ca^{2+} storage organelle (Sandow, 1965; Beeler and Reuter, 1970). The transduction mechanisms that link T-tube depolarization and SR Ca^{2+} release in skeletal and cardiac muscle are quite different. In cardiac muscle, T-tube depolarization activates the L-type Ca^{2+} channel, resulting in a small Ca^{2+} influx that activates the SR Ca^{2+} release channel (Fabiato, 1983; Beuckelmann and Wier, 1988; Näbauer et al., 1989). This transduction mechanism in cardiac muscle is commonly referred to as Ca^{2+}-induced Ca^{2+} release (CICR). In skeletal muscle, the transduction mechanism is not dependent on Ca^{2+} influx across the T-tube membrane (Caputo, 1968; Armstrong et al., 1972; Miledi et al., 1977). Instead, T-tube depolarization is thought to be sensed by voltage-sensing proteins, and then this information is relayed through a physical protein-protein link to the SR Ca^{2+} release channel (Schneider and Chandler, 1973; Shirokova et al., 1996). Thus the T-SR transduction mechanism in cardiac muscle involves a diffusing second messenger (i.e., Ca^{2+}), while the T-SR transduction mechanism in skeletal muscle involves a direct physical link.

The study of intracellular Ca^{2+} signaling in isolated skeletal and cardiac muscle cells has a long, distinguished, and productive history. Traditionally, these studies used a wide array of clever but invasive experimental approaches. For example, intracellular Ca^{2+} signaling in skeletal muscle has been well defined in highly stretched, cut fiber segments (Hille and Campbell, 1976; Vergara et al., 1978; Kovacs et al., 1979). Intracellular Ca^{2+} signaling in cardiac muscle has been elegantly defined in mechanically skinned myocytes (Fabiato, 1983). Traditionally, the SR Ca^{2+} release process is triggered by a wide array of nonphysiological perturbations (i.e., ionic exchange, voltage-clamp steps, and/or pharmacological agents like caffeine). The use of nonphysiological invasive experimental manipulations is well justified because it is difficult to accurately quantitate local intracellular Ca^{2+} signals in moving intact cells. The consequence is that the spatiotemporal distribution of local intracellular SR Ca^{2+} release in contracting cells at normal resting sarcomere lengths in the absence of potentially invasive experimental manipulations has not been well defined. This is unfortunate because this information is fundamental to delineating the constraints that govern intracellular Ca^{2+} release and distribution under normal physiological conditions.

The blurring produced by the mechanical movement (i.e., contraction) and/or diffusion represents a persistent experimental obstacle to fluorescence imaging of local intracellular Ca^{2+} in muscle cells. To overcome this, a series of high-resolution snapshot images of Rhod-2 fluorescence were taken during very brief (7 ns) flashes of excitation light from a frequency-doubled Nd:YAG laser. Each snapshot image is essentially an instantaneous freeze-frame picture of the Ca^{2+} profile in the cell during the flash. Blurring artifacts are minimized because there is no significant cell shortening or molecular diffusion during the brief 7-ns flash. Precisely timed flashes during successive APs re-

Received for publication 28 April 1999 and in final form 24 September 1999.

Address reprint requests to Dr. Ariel L. Escobar, Instituto Venazolano de Investigaciones Científicas, Centro de Física Carretara Panamericana Km 11 Pipe, Venezuela. Tel: 582-504-1369; E-mail: aescobar@cbb.ivic.ve.

0006-3495/00/01/164/10 $2.00

vealed the spatiotemporal distribution of local intracellular SR Ca^{2+} release in contracting muscle cells in two spatial dimensions at high temporal resolution.

METHODS

Cardiac muscle preparation

Rat ventricular myocytes were enzymatically dissociated with the Langendorff retroperfusion technique (Mitra and Morad, 1985). Briefly, the heart was removed and placed on a petri dish containing a Ca^{2+}-free Tyrode ($Tyrode_{noCa}$) solution containing 140 mM NaCl, 5.4 mM KCl, 1 mM $MgCl_2$, 0.33 mM NaH_2PO_4, 10 mM HEPES, and 10 mM glucose, pH 7.4, at 37°C. Then the aorta was cannulated and the coronary arteries were washed with $Tyrode_{noCa}$ solution for 6 min. The heart was then perfused with $Tyrode_{noCa}$ solution containing 2 mg/ml collagenase (Worthington Biochemical Corporation, Lakewood, NJ; 257 U/mg) and 0.1 mg/ml protease (Pronase E; Sigma, St. Louis, MO; 4.4 U/mg). The dissociation procedure was concluded by perfusing the heart with Tyrode solutions containing 0.2 and then 2 mM $CaCl_2$. The dissociated cells were used the same day.

Skeletal muscle preparation

Single skeletal muscle fibers were obtained from the lumbricalis muscles of the tropical frog *Leptodactylus insularis*. Whole muscles were incubated in Ringer's solution containing 115 mM NaCl, 2.5 KCl, 1.8 $CaCl_2$, 5 HEPES (pH 7.3), and 8 mg/ml collagenase (Worthington Biochemical Corporation; 257 U/mg) at 37°C for 35 min. Removing the collagenase and adding 5 mg/ml bovine serum albumin stopped the fiber dissociation process. Fibers were mechanically separated with a Pasteur pipette tip and placed on a coverslip at slack length for experimentation.

Optical measurements

Isolated cardiac and skeletal muscle cells were loaded with Rhod-2 (Molecular Probes, Eugene, OR) by incubation in a 10 μM Rhod-2/AM solution for 30–60 min at room temperature. After Rhod-2 loading, cells were rinsed continuously for 15 min. The loaded washed cells were then placed on the stage of an inverted fluorescence microscope (Nikon Diaphot, Tokyo, Japan) modified for flash laser imaging (Escobar et al., 1994). All experiments were carried out at room temperature. Action potentials were triggered by field stimulation using micropositioned platinum wires. A Zeiss planapo 63× (NA 1.4) oil immersion objective was used to image the cells. Snapshot images were obtained by epiilluminating a relatively large field on the cell with a single 7-ns-duration, 532-nm light flash from a frequency-doubled Nd-YAG laser (Spectra Physics, Mountain View, CA). The size of the illuminated field was defined by the magnification of the objective and the size of the aperture through which the excitation light was directed.

Images of the illuminated area were acquired with a cooled CCD camera (MCD 600; Spectra Source, Ventura, CA). Image collection was synchronized to electrical stimulation. Individual images were collected after precisely timed delays from the electrical stimulus. The delay between the electrical stimulus and image acquisition was digitally mastered with the computer hardware. The synchronization of laser, the CCD camera, and the A/D conversion system was controlled with a LabVIEW (National Instruments, Austin, TX)-based computer program.

The inherent blurring of fluorescent images (confocal or not) makes it difficult to precisely define local (submicron) Ca^{2+} gradients. Thus no formal attempt was made to define the submicron Ca^{2+} gradients here. The intention of our study was not to precisely define the amplitude of the subsarcomeric Ca^{2+} gradients detected. Instead, our intent was to show that clear differences exist in contracting cardiac and skeletal muscle cells at similar sarcomere lengths. To thoroughly and formally define subsarcomeric Ca^{2+} gradients would require confocal spatial resolution combined with the temporal resolution of laser flash microscopy.

Image analysis

Line scan measurements were made on digital images with the aid of the Scion Image analysis program (Scion Corp., Frederick, MD). One-dimensional fast Fourier transforms (FFTs) were implemented on 128 line scan measurements of 128 pixels, using the FFT algorithm provided in the Origin 5.0 software package (Microcal, Northampton, MA). The polar forms of the FFT of each line scan were averaged and plotted for different snapshot images at different times during the fluorescent transients.

Mathematical modeling of Ca^{2+} distribution

To theoretically simulate the myoplasmic free Ca^{2+} concentration changes that may occur during a twitch, a multicompartment unidimensional diffusion model was evaluated (Cannell and Allen, 1984; Pizarro et al., 1991). The model consists of a segmented hemisarcomere cut into n slices. In our modeling, n was equal to 12. The first slice (compartment 0) was presumed to be the site of the Ca^{2+} input flux (i.e., the junctional space). Free Ca^{2+} concentration changes in all compartments were calculated as the influx into minus the efflux out of the compartment. Formally,

$$\frac{\partial[Ca^{2+}](t, i)}{\partial t} = J_{in}(t, i) - J_{out}(t, i)$$

where t is time, J is the directional flux, and i is the segment number. The Ca^{2+} influx component was assumed to arise from three different sources: 1) SR Ca^{2+} release, 2) unbinding of Ca^{2+} from known buffers, and 3) Ca^{2+} flux from neighboring compartments. The Ca^{2+} influx due to SR Ca^{2+} release was governed by the Ca^{2+} gradient across the SR membrane and SR Ca^{2+} release channel function. The Ca^{2+} influx due to Ca^{2+} unbinding from known buffers included known endogenous Ca^{2+} binding proteins (e.g., parvalbumin) and the exogenously added Ca^{2+} indicator Rhod-2. The Ca^{2+} efflux component was also assumed to arise from different sources: 1) SR Ca^{2+} reuptake and Ca^{2+} binding to known buffers and 2) Ca^{2+} flux into neighboring compartments. It was assumed that the SR Ca^{2+} reuptake process did not take place in the junctional segments. The SR Ca^{2+} reuptake was assumed to be active Ca^{2+} transport, the maximum rate and kinetics of which were defined by a second-order kinetic scheme. The only entity allowed to diffuse is the Ca^{2+} ion. All equations were numerically integrated using a finite-difference approximation (Euler method), with the aid of the Scope 3.5 simulation package.

The Ca^{2+} release waveforms that were used to drive the model were obtained from the experimental data. Skeletal and cardiac simulations were driven with the measured skeletal and cardiac Ca^{2+} release waveforms, respectively. Thus differences in the rate of SR Ca^{2+} release in skeletal and cardiac muscle are considered in the modeling. Recently it was demonstrated that the rate of SR Ca^{2+} release is not affected by the rate of SR Ca^{2+} uptake (Caputo et al., 1999). Thus differences in uptake rate were not considered here. It is clear that intracellular Ca^{2+} buffer capacity is very important and will have an impact on whether subsarcomeric Ca^{2+} gradients can be detected (Cleeman et al., 1998). Higher Ca^{2+} buffer capacity would make it easier to detect gradients. Skeletal muscle has higher Ca^{2+} buffer capacity than cardiac muscle because of the presence of parvalbumin. Our skeletal muscle simulations take this into consideration, as Ca^{2+} binding and Mg^{2+} binding to parvalbumin are included. Simulations using skeletal parameters (including parvalbumin) and either the cardiac or skeletal Ca^{2+} release waveforms were performed (data not shown). These simulations revealed that the presence of higher buffer capacity was not sufficient to generate detectable gradients when the slower Ca^{2+} release

waveforms were used. The skeletal and cardiac simulations shown in this study were carried out using skeletal or cardiac parameters, respectively. The parameters used are listed in Table 1.

RESULTS

Intracellular Ca^{2+} distribution in intact cardiac myocytes

Intact rat ventricular cardiac myocytes were isolated and loaded with the fluorescent Ca^{2+} indicator Rhod-2. An image of transilluminated rat cardiac ventricular myocyte is shown in Fig. 1 *A* (*left*). The striations (~2 μm apart) arising from the ordered arrangement of the contractile proteins of the sarcomere were clearly evident. A snapshot image of the same cell taken 70 ms after an AP was triggered by field stimulation is also shown in Fig. 1 *A* (*right*). The pair of images in Fig. 1 *A* illustrates the relationship between cell morphology and image area. Note that the image area, the area illuminated by excitation light, represents only a portion of the entire cell.

A series of snapshot images taken at different times after an AP was triggered is shown in Fig. 1 *B*. Before the AP, the relatively low resting fluorescence indicates that the indicator was homogeneously distributed and that there was a relatively low resting Ca^{2+} level (~100 nM). After the AP, an elevation in intracellular Ca^{2+} concentration was first evident at the 10-ms mark. The AP-triggered Ca^{2+} release nearly reached peak intensity at the 70-ms mark. Some heterogeneity in the Ca^{2+} distribution during the release process was evident. This heterogeneity, however, could not be clearly correlated with any morphological determinant like sarcomere spacing. Thus our snapshot imaging approach was unable to reliably detect any subsarcomere Ca^{2+} gradients during the AP-triggered Ca^{2+} release process. This was disappointing because subsarcomere Ca^{2+} gradients must arise if Ca^{2+} is released rapidly at the T-SR junction and then slowly diffuses across the sarcomere. Nevertheless, the overall AP-triggered Ca^{2+} transient ($\Delta F/F$) in the cardiac myocyte was reconstructed from several snapshot images (Fig. 1 *C*). The reconstructed Ca^{2+} transient contains points that are not represented in Fig. 1 *B*. The temporal characteristics of the AP-triggered Ca^{2+} transient were nearly identical at all points in the snapshot image. The AP triggered a rapid Ca^{2+} rise that spontaneously decays over several hundred milliseconds. The rise time of the AP-triggered Ca^{2+} transient in the cardiac myocyte had a time constant of 16.4 $\pm$ 0.71 ms (mean $\pm$ SEM).

The same experiment was performed on single frog skeletal muscle fibers. The sarcomere length of the skeletal fibers was nearly identical to that of the cardiac myocytes tested above. The sarcomere lengths of a typical cardiac myocyte and skeletal muscle fiber are compared in the transillumination images shown in Fig. 2. Sarcomere length in cardiac and skeletal muscle cells corresponds to the distance between transverse tubules. This distance is important because SR Ca^{2+} release occurs at the junction (i.e., the T-SR junction). All cells tested (cardiac or skeletal) had a

TABLE 1 Modeling parameters

Parameter	Cardiac case	Skeletal case
Sarcomere spacing	2 μm	2 μm
Sarcomere cross-sectional area	0.8 μm^2	0.8 μm^2
Volume of sarcoplasmic reticulum (SR)	0.2 μm^3	0.2 μm^3
Ca^{2+} diffusion coefficient	0.150 $\mu m^2 ms^{-1}$	0.150 $\mu m^2 ms^{-1}$
Ca^{2+} indicator: concentration	30 μM	30 μM
Ca^{2+} indicator: dissociation constant	18 μM	18 μM
Ca^{2+} indicator: association rate	0.1 $\mu M^{-1} ms^{-1}$	0.1 $\mu M^{-1} ms^{-1}$
Ca^{2+} buffer: concentration	700 μM	700 μM
Buffer: Ca^{2+} dissociation constant	5 nM	5 nM
Buffer: Ca^{2+} association rate constant	0.002 $\mu M^{-1} ms^{-1}$	0.002 $\mu M^{-1} ms^{-1}$
Buffer: Mg^{2+} dissociation constant	∞	91 μM
Buffer: Mg^{2+} association rate constant	0	0.000066 $\mu M^{-1} ms^{-1}$
Free Ca^{2+} concentration (at rest)	0.1 μM	0.1 μM
Free Mg^{2+} concentration (at rest)	1 mM	1 mM
Troponin: concentration	140 μM	140 μM
Troponin: Ca^{2+} dissociation constant	0.25 μM	0.25 μM
Troponin: Ca^{2+} association rate	0.001 $\mu M^{-1} ms^{-1}$	0.001 $\mu M^{-1} ms^{-1}$
Intra-SR Ca^{2+} buffer: concentration	30 mM	30 mM
Intra-SR Ca^{2+} buffer: dissociation constant	1 mM	1 mM
Intra-SR Ca^{2+} buffer: association rate	0.002 $\mu M^{-1} ms^{-1}$	0.002 $\mu M^{-1} ms^{-1}$
Intra-SR free Ca^{2+} concentration	500 μM	500 μM
Maximum SR Ca^{2+} release rate	0.03 $\mu M ms^{-1} \mu m^2$	0.03 $\mu M ms^{-1} \mu m^2$
Maximum SR Ca^{2+} pump rate	0.1 $\mu M ms^{-1} \mu m^2$	0.1 $\mu M ms^{-1} \mu m^2$
SR pump Ca^{2+} dissociation constant	1 μM	1 μM
SR pump Ca^{2+} association rate	0.01 $\mu M^{-1} ms^{-1}$	0.01 $\mu M^{-1} ms^{-1}$

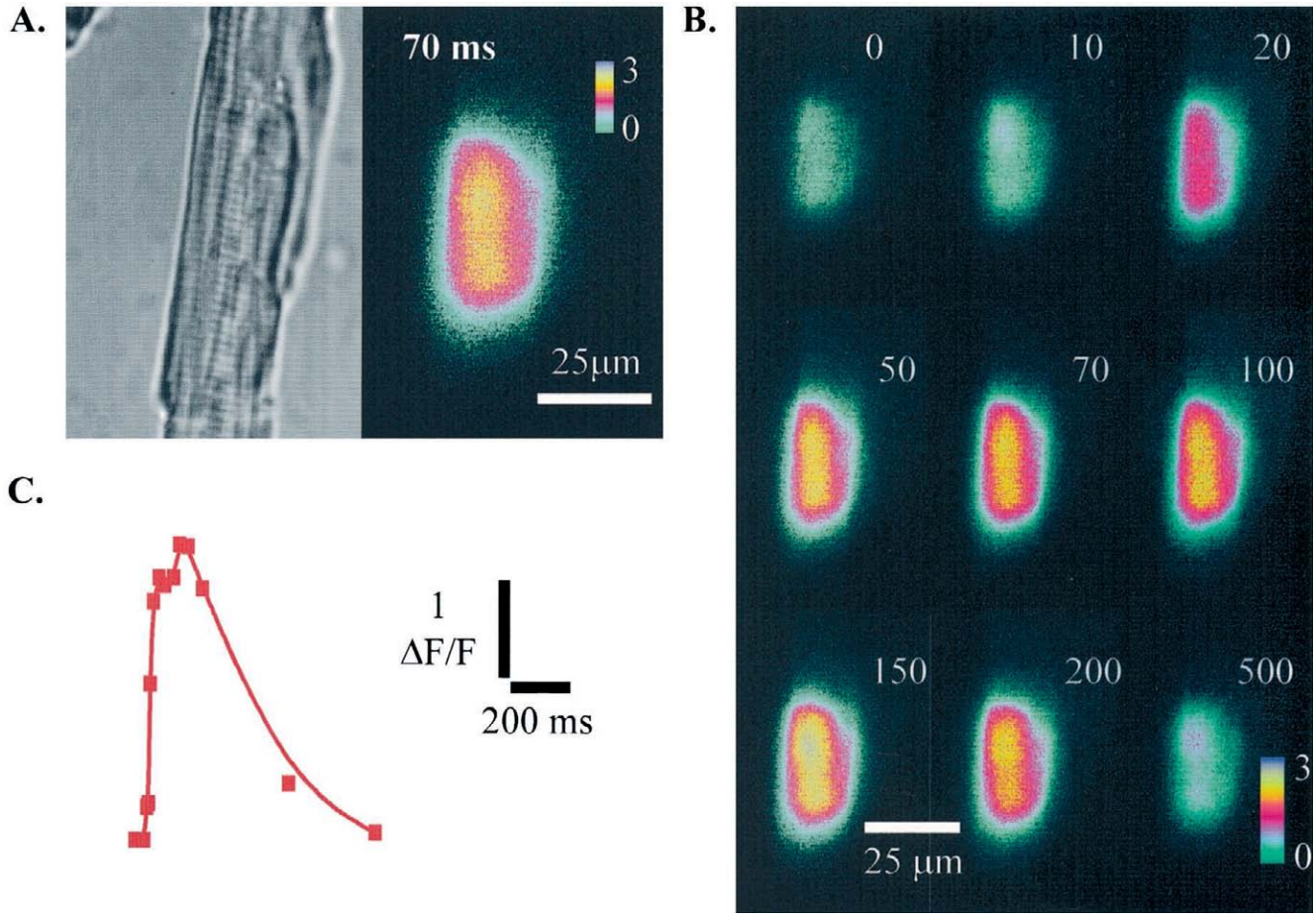

FIGURE 1 (*A*) A transillumination image of a rat ventricular cardiac myocyte (*left*) and a single 7-ns exposure fluorescence image (i.e., snapshot image) of the same cell taken 70 ms after field stimulation (*right*). The field stimulation induced an action potential (AP) on the surface membrane of the cell. These data are representative of 27 similar experiments. (*B*) Sequence of snapshot images of a rat ventricular cardiac myocyte taken at different times along the AP-induced Ca^{2+} transient. One image was taken at the specified delay after each field stimulus. The series of images represent data collected on successive APs. The pseudo-color scale corresponds to $\Delta F/F$ measurements. (*C*) The fluorescent signal obtained from the same point in the cell at different delays from the field stimulation are plotted as a function of time.

sarcomere spacing of ~2 μm ($\pm$ 0.2 μm). Thus the SR Ca^{2+} release sites were equally spaced along the length of the cells.

Like the cardiac myocytes, the intact skeletal muscle fibers were loaded with the fluorescent Ca^{2+} indicator Rhod-2. A segment of a typical skeletal muscle fiber is shown in Fig. 3 *A* (*left*). A snapshot image of the same fiber taken 2.5 ms after an AP was triggered by field stimulation is shown in Fig. 3 *A* (*right*). Like the cardiac data, the snapshot image area represents only a portion of the skeletal muscle fiber. The image area is the region of the cell illuminated by the 7-ns-long flash of excitation light. Heterogeneity in the free Ca^{2+} distribution at the 2.5-ms mark is evident. The heterogeneity is in the form of transverse high- and low-intensity fluorescence bands that repeat regularly along the length of the cell. This banding (Fig. 3 *A*, *right*) corresponds well to the sarcomere spacing of the cell observed in the transillumination image (Fig. 3 *A*, *left*).

A series of snapshot images taken at selected times after an AP was triggered is shown in Fig. 3 *B*. Before the AP, the uniform resting fluorescence of the Rhod-2-loaded cell suggests relatively even indicator distribution and a low resting Ca^{2+} level (~100 nM). Intracellular Ca^{2+} release was evident 0.5 ms after the AP was triggered. The AP-triggered Ca^{2+} release reached peak intensity at the 6-ms mark. Periodic distinct regions of high and low Ca^{2+} concentration (i.e., high- and low-intensity fluorescence bands) were evident for the first 4 ms after the AP. The fluorescent banding becomes more and more marked as time progresses. This in part reflects the inherent signal-to-noise characteristics of the detection system. At early times, the amount of Ca^{2+} release is small and near the limit of resolution. Maximum subsarcomeric Ca^{2+} gradients occur at the peak of the Ca^{2+} release and later on (i.e., at the 2.5-ms mark). The appearance of Ca^{2+} gradients within a few milliseconds indicates a high synchrony of release.

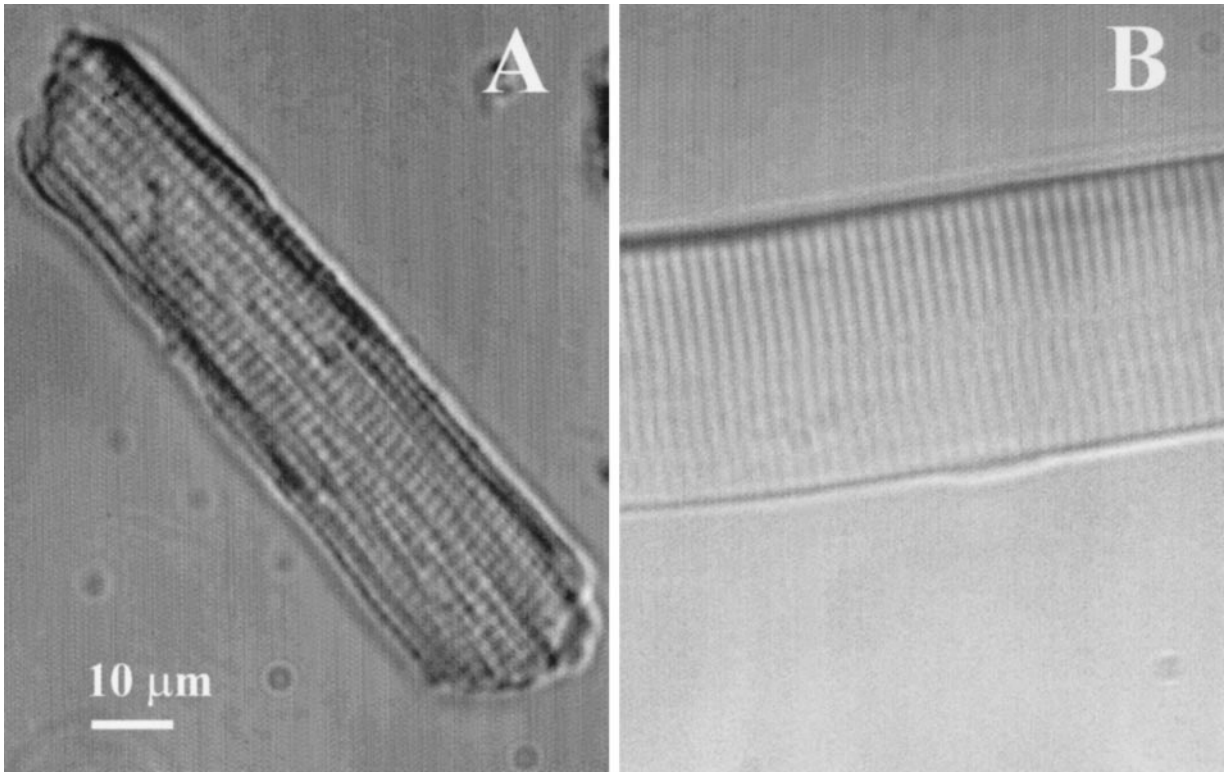

FIGURE 2 Structural comparison between a rat ventricular cardiac myocyte (*A*) and a single lumbricalis frog skeletal muscle fiber (*B*). Transillumination images show that the two cell types have a similar sarcomere length (~2 μm).

Escobar et al. (1994) demonstrated a similar pattern of intracellular Ca^{2+} release in highly stretched skeletal muscle fibers (sarcomere length ~4 μm). These authors argued that the bands of high Ca^{2+} concentration (i.e., the regions of high fluorescence intensity) correspond to the position of the T-tube SR junction and that the bands of low Ca^{2+} concentration correspond to the interjunctional space. If this interpretation is equally valid here, then our data illustrate that significant subsarcomeric Ca^{2+} gradients occur in response to an AP in contracting skeletal muscle fibers at normal resting sarcomere lengths (~2 μm).

The reconstructed fluorescence transient ($\delta F/F$) from several snapshot images is illustrated in 3 *C*. This transient represents the fluorescence intensity at the T-SR junction (i.e., site of SR Ca^{2+} release). The AP triggered a very rapid Ca^{2+} rise (time constant 0.85 ± 0.23 ms) that spontaneously decayed with a time constant of 10.8 ± 3.7 ms (mean ± SEM). These values are ~20 times faster than those measured in cardiac cells. The data in Fig. 3 illustrate the relatively high spatial and temporal resolution of the snapshot imaging method applied. For example, the high- and low-fluorescence banding (Fig. 3 *A, right*) demonstrates submicron (*x-y*) spatial resolution. The high number of points on the rising phase of the Ca^{2+} transient (Fig. 3 *C*) demonstrates submillisecond temporal resolution. The point is that the applied snapshot imaging method has the capacity to detect subsarcomeric Ca^{2+} gradients at a sarcomere spacing of 2 μm. Thus the absence of subsarcomeric Ca^{2+} gradients during AP-triggered Ca^{2+} release in cardiac myocytes (Fig. 1) is not due to the resolving power of the imaging system.

To quantitate the spatial fluorescence banding, the fluctuations in intensity along lines perpendicular to the Z-lines were analyzed using the fast Fourier transform (Fig. 4). The profile of fluorescence intensity along a line perpendicular to the sarcomeres (i.e., z-lines) in a skeletal and cardiac muscle is illustrated in Fig. 4 *A*. The skeletal and cardiac data were collected 2.5 ms and 100 ms after electrical stimulation, respectively. These plots of line intensity have two fundamental features. First, there is lower intensity at the ends of the plots because of the finite size of the illuminated circular spot. Second, the variance in the signal is substantially greater in the skeletal muscle case. This greater variance is generated by the distinct fluorescence gradients that occur along the line in skeletal muscle. The variance in the cardiac case is smaller because of the absence of big fluorescence gradients. To provide a more quantitative description of the size and periodicity of the fluorescence gradients, a one-dimensional fast Fourier analysis of 128 of these line scan measurements was made in both the skeletal and cardiac cases. The results of this Fourier analysis are shown in Fig. 4 *B*. Each of the four

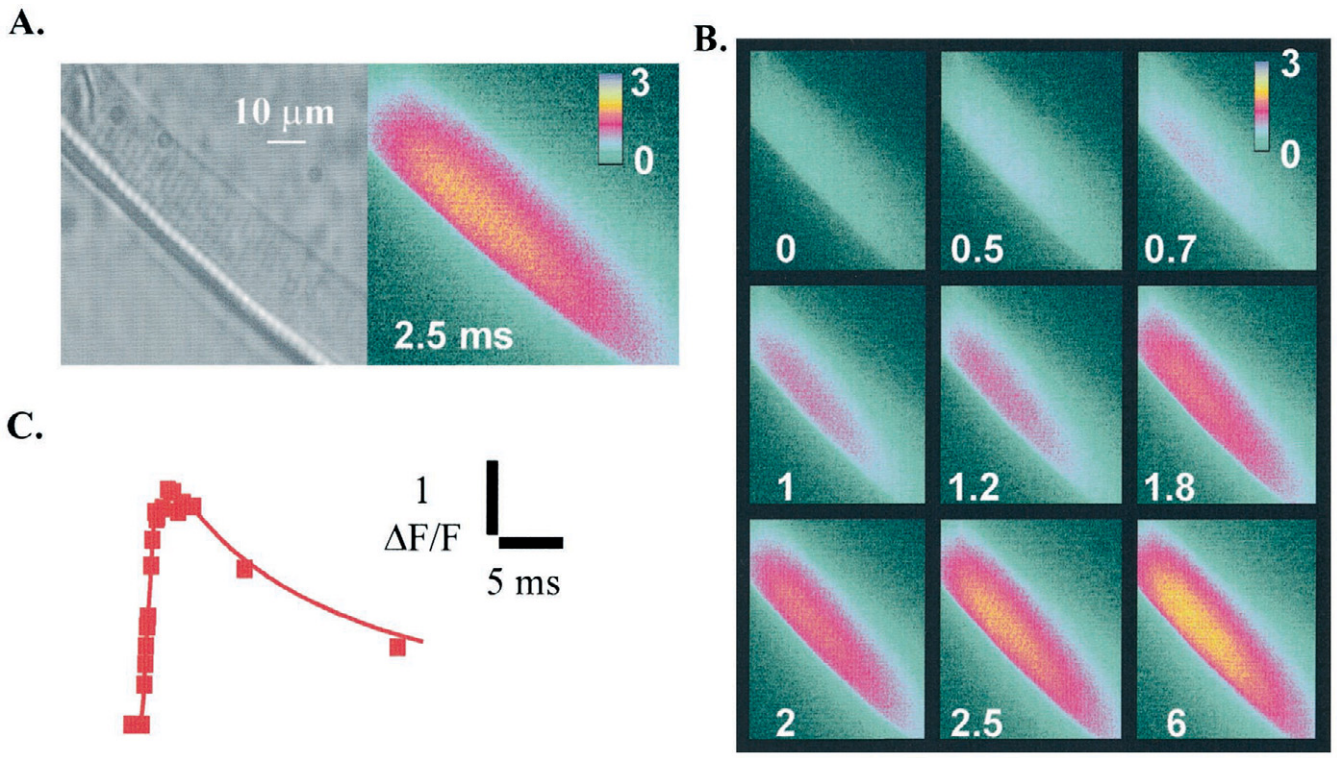

FIGURE 3 (*A*) Transillumination image of a single lumbricalis fiber (*left*) and the corresponding snapshot image of the same cell (*right*) taken 2.5 ms after field stimulation. These data are representative of 22 similar experiments. Note that a larger area of the skeletal fiber is illuminated than in the cardiac case. (*B*) Sequence of snapshot images of a single lumbricalis fiber taken at different delays after field stimulation. One image was taken at the specified delay after each field stimulus. The series of images represent data collected on successive APs. Strong subsarcomeric Ca^{2+} gradients were observed during the first 4 ms of the AP-induced Ca^{2+} transient. (*C*) The fluorescent signal obtained from the same point in the cell is plotted as a function of time.

plots (skeletal at left, cardiac at right) shows the modulus of the average polar fast Fourier transform. In all plots, there are high values at the zero frequency point, and this corresponds to the average fluorescence signal along the scan line. Interestingly, a small but distinct second peak (*arrows*) becomes evident only in the skeletal muscle case. This second peak occurs at the 1.8-ms and 2.5-ms time points at the 0.6-μm^{-1} mark. This corresponds to a mean periodicity of fluorescence intensity occurring every 1.7 μm (i.e., 1/0.6 μm^{-1}). Note that this second peak was absent at the 0.5-ms and 6-ms time points because there are no clear subsarcomeric gradients at those times. This analysis also shows that the biggest global fluorescence signal (i.e., the "DC" level of the FFT) occurred at the 6-ms point, but the most distinct gradients occurred at the 2.5-ms point. The absence of a distinct second peak in the cardiac muscle case is consistent with the absence of a detectable subsarcomeric Ca^{2+} gradient in those cells.

Our inability to detect subsarcomeric Ca^{2+} gradients in cardiac muscle does not mean that they do not exist. In fact, our interpretation is that subsarcomeric Ca^{2+} gradients do indeed exist in the cardiac cells, but those subsarcomeric Ca^{2+} gradients are simply more difficult to resolve. Several factors may contribute to the difficulty of detecting subsarcomeric Ca^{2+} gradients in the cardiac cells. For example, the distribution of the fluorescent Ca^{2+} indicator (Rhod-2) could be different in the cardiac and skeletal muscle cells. The spacing of SR Ca^{2+} release sites along the length of the cell could be different. The axial (z axis) alignment of sarcomeres in cardiac cells may not be as tight as that in skeletal muscle fibers. These possibilities are addressed by the experimental data. The relatively uniform resting fluorescence of the Rhod-2-loaded cells suggests that the indicator was evenly distributed in both the cardiac and skeletal cells. Similar sarcomere lengths suggest similar spacing of SR Ca^{2+} release sites along the length of the cells. Although periodic sarcomere registration shifts can been seen in the cardiac cells (Fig. 2), these shifts do not occur frequently enough to explain the absence of detectable subsarcomeric Ca^{2+} gradients. However, other possible factors that may contribute to the difficulty of detecting subsarcomeric Ca^{2+} gradients in the cardiac cells cannot be easily addressed, for example, endogenous cytosolic Ca^{2+} buffers that may be differentially and nonuniformally distributed along the cardiac or skeletal muscle sarcomere. Differences in ultrastructure could explain the different results in cardiac and skeletal muscle (Soeller and Cannell, 1999). Mitochondria and nuclei are sandwiched in and among the contractile apparatus in cardiac muscle, generating ultrastructural irregularities that could have an impact on local Ca^{2+}

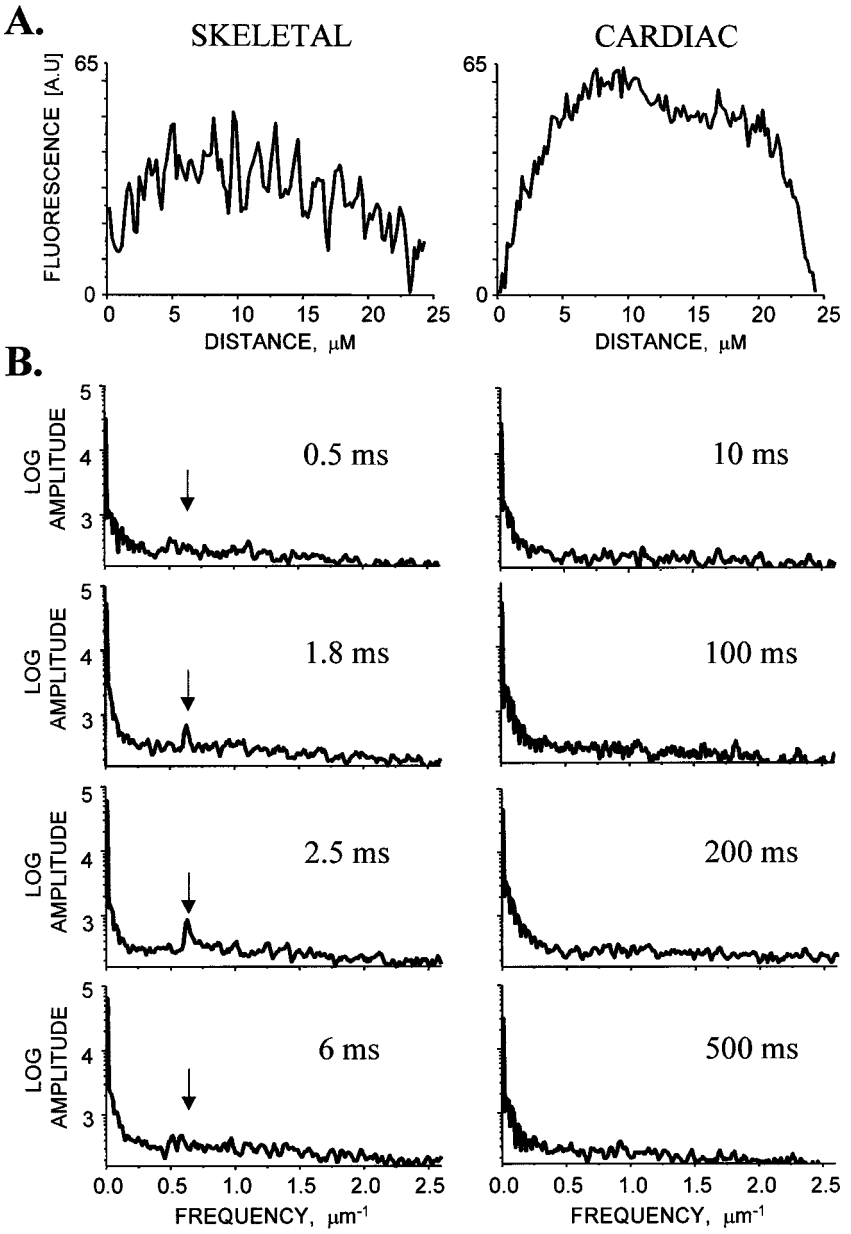

FIGURE 4 (*A*) Line scan plots of fluorescence intensities of a skeletal fiber (*left*; 2.5 ms after stimulus) and a cardiac ventricular myocyte (*right*; 100 ms after stimulus). Lines were drawn perpendicular to the *z* lines. Note the large variance of the signals. (*B*) Average one-dimensional fast fourier transform (FFT) of 128 line scan recordings of 128 pixels obtained from a skeletal fiber (*left plots*) or cardiac cell (*right plots*) at four different times during a fluorescent transient. The arrow denotes the intensity peak corresponding to $>1.7\ \mu m$ ($1/0.6\ \mu m^{-1}$).

imaging. The point is that potential alternative explanations should be acknowledged. Perhaps the simplest explanation for our results is described below.

The absence/presence of detectable subsarcomeric Ca^{2+} gradients in cardiac/skeletal muscle cells may simply be the result of the different mechanisms that link T-tube depolarization to the SR Ca^{2+} release process. In skeletal muscle, the brief AP (~2 ms) results in almost synchronous activation of SR Ca^{2+} release sites across the muscle fiber. In contrast, the CICR process in cardiac cells involves a relatively slow Ca^{2+} diffusion step and the recruitment of multiple SR Ca^{2+} release sites. To evaluate this possibility, a very simple diffusional model (see Methods) was used to predict subsarcomeric Ca^{2+} distributions that may arise in response to different Ca^{2+} release functions (Fig. 5). The model was driven by a measured cardiac or a skeletal Ca^{2+} release waveform. The time courses of the driving Ca^{2+} release functions and simulated snapshot images are illustrated. Both the cardiac (Fig. 5 *A*) and skeletal (Fig. 5 *B*) Ca^{2+} release functions generate subsarcomeric Ca^{2+} gradients. In the cardiac case (Fig. 5 *A*), the peak Ca^{2+} levels are relatively small compared to the mean Ca^{2+} level. In contrast, the same simple distributed spatial model driven by the measured skeletal Ca^{2+} release waveform predicts large distinct subsarcomeric Ca^{2+} gradients. Thus the absence/presence of detectable subsarcomeric Ca^{2+} gradients in cardiac/skeletal muscle cells may simply be due to the different kinetics of the free Ca^{2+} input signals in each case.

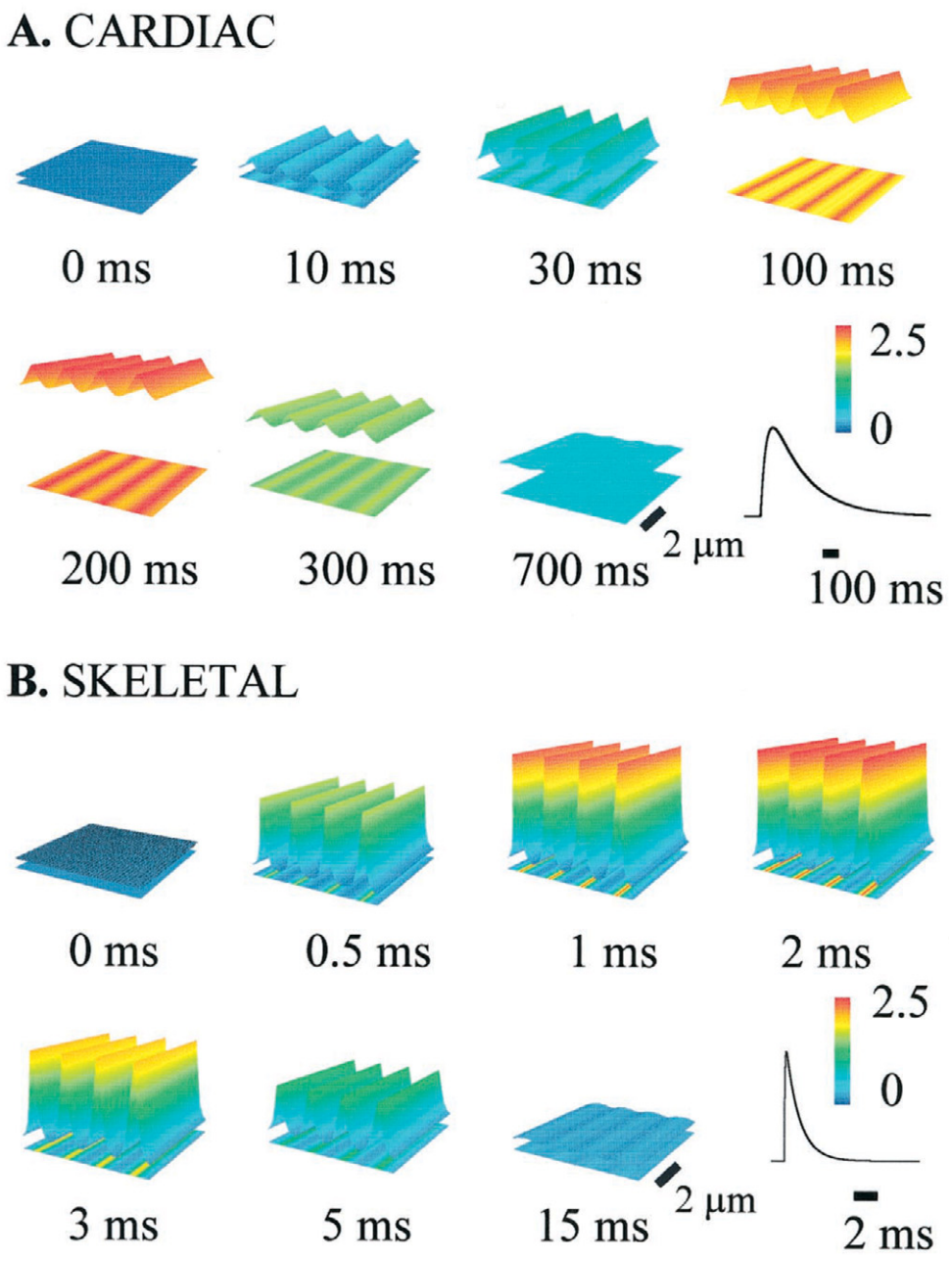

FIGURE 5 Simulated temporal and spatial fluorescence distribution according to our diffusion model. (*A*) Snapshot image simulations during a Ca^{2+} transient when the model was driven by an SR Ca^{2+} flux derived from our measured cardiac Ca^{2+} release data. (*B*) Snapshot image simulations when the model was driven by SR Ca^{2+} flux derived from our measured skeletal Ca^{2+} release data. Note the large difference in time course between the cardiac and skeletal cases. The parameters used in the model are listed in Table 1. Note that maximum rates of release and uptake do not necessarily correspond to flux because the flux depends on many factors (i.e., gradient direction, dissociation constant, association rate). The concentration of intracellular Ca^{2+} buffer (700 μM) and its kinetics was obtained from the literature (Cannell and Allen, 1984).

DISCUSSION

The snapshot laser imaging strategy

In this paper we demonstrate that single snapshot fluorescent images can be taken at the time scale of the decaying lifetime of a fluorescent indicator (Rhod-2) in a living cell. The lifetime of most commercially fluorescent Ca^{2+} indicators is on the order of 2–5 ns. In this study, fluorescent images were acquired during a 7-ns flash of excitation light. Thus the fluorescent signals detected by our CCD camera essentially represent the integration of the lifetime relaxation of the fluorophor. Another feature of the applied snapshot imaging strategy is that it minimizes diffusion and movement artifacts because 7 ns is simply not enough time for a moving particle to blur the image. Thus the snapshot method provides the means to generate "freeze-frame" fluorescence images of local Ca distributions in moving muscle cells. Traditional imaging strategies would require invasive experimental manipulation to restrict movement or be limited to measurements before movement occurs.

A clear disadvantage of the snapshot imaging strategy is that it is not confocal (Monck et al., 1994). A conventional scanning confocal microscope has slightly better spatial resolution. This disadvantage is somewhat offset by higher temporal resolution and the ability to collect spatial information in two dimensions simultaneously. The traditional

conventional scanning confocal microscope operates at its optimal temporal resolution (i.e., line scan mode) at the expense of spatial information (i.e., data collected in only one spatial dimension).

Ca^{2+} distributions in ventricular cardiac myocytes and skeletal muscle fibers

The SR Ca^{2+} release machinery in cardiac and that in skeletal muscle cells share many common features. For example, T-SR communication is mediated by dihydropyridine and ryanodine receptors in both tissues, albeit by different mechanisms. The architecture of the T-SR junction is similar. The spacing of SR Ca^{2+} release sites along the length of the cell is similar. Such striking morphological similarities could imply a common function. However, our data show that cellular architecture is not the only determinant of the local intracellular Ca^{2+} signaling. Subsarcomeric Ca^{2+} gradients were detected in skeletal muscle fibers (Fig. 3) but not in cardiac myocytes (Fig. 1). This is significant because the sarcomere length was constant (i.e., similar SR Ca^{2+} release machinery spacing) between the two cell types and the measurements were made under nearly ideal physiological conditions (i.e., APs instead of voltage clamp steps, low Ca^{2+} indicator level with no other exogenous Ca^{2+} buffer added), with the cell free to contract.

The absence/presence of a subsarcomeric Ca^{2+} gradient in cardiac/skeletal muscle cells (respectively) is most likely due to the marked differences in the synchrony of SR Ca^{2+} release activation. For example, it is thought that AP-triggered SR Ca^{2+} release is highly synchronized across the skeletal muscle cell. A highly synchronized Ca^{2+} release at the T-SR junction could generate the observed subsarcomeric Ca^{2+} gradients if Ca^{2+} diffusion into the nonjunction space is significantly slower than T-SR signal transduction and Ca^{2+} release processes combined. Previously we have shown that the dissipation of subsarcomeric Ca^{2+} gradients in stretched skeletal muscle fibers (i.e., sarcomere $\sim 4\ \mu m$) were apparent for nearly 12 ms after triggering by an AP (Escobar et al., 1994; Monck et al., 1994). Here we observed that subsarcomeric Ca^{2+} gradients in skeletal muscle fibers at a sarcomere length of $\sim 2\ \mu m$ were evident for only $\sim$3–4 ms. The diffusion time in one dimension varies with the square of the distance. Thus doubling distance (2 versus 4 μm) would theoretically increase the diffusion time by about fourfold (3 versus 12 ms). Thus diffusion could explain the temporal redistribution of Ca^{2+} in skeletal muscle fibers reported here and in the previous studies.

In the cardiac myocytes, subsarcomeric Ca^{2+} gradients were not evident, but this does not mean that they did not exist. Two groups have in fact reported subsarcomeric Ca^{2+} gradients in isolated cardiac myocytes (Isenberg et al., 1996; Cleeman et al., 1998). Isenberg et al. (1996) reported the presence of small but detectable subsarcomeric Ca^{2+} gradients in guinea pig ventricular myocytes driven by fast voltage clamp steps after a complex digital manipulation of multiple images. Cleeman et al. (1998) reported subsarcomeric Ca^{2+} gradients in voltage-clamped ventricular myocytes. In the latter study, a very high concentration of indicator and the presence of 5 mM EGTA eliminated contraction and limited Ca^{2+} diffusion out of the junctional region, facilitating the detection of gradients. In our study, cells were triggered to contract by an action potential; thus the rate of SR Ca^{2+} release was not artificially accelerated or synchronized by a fast voltage clamp step. Furthermore, our studies involved single raw images taken in the presence of only 50 μM exogenous Ca^{2+} buffer (i.e., the indicator). Under these conditions, no subsarcomeric Ca^{2+} gradients were detected in cardiac myocytes. The inability to resolve subsarcomeric Ca gradients does not necessarily mean our results are in conflict with those of others. It may simply be that in the absence of certain nonphysiological manipulations the gradients are difficult to detect.

Recently the elegant work of Soeller and Cannell (1999) clearly showed that T-tubule topology in the rat ventricular myocyte is much more complex than previously thought. This could have an impact on the interpretation of our results. The presence of less ordered T-tubule arrays may imply that SR Ca^{2+} release site topology may not be highly ordered. This could geometrically smear the subsarcomeric Ca gradients and explain why gradients were not detected in cardiac muscle. However, two laboratories have detected subsarcomeric Ca^{2+} gradients in cardiac muscles under certain experimental conditions (Isenberg et al., 1996; Cleeman et al., 1998). The point is that the presence of gradients in those studies implies that topology of SR Ca^{2+} release sites in cardiac muscle must be highly ordered. It might be that not all regions of the T-tubule form T-SR junctions. The T-SR junctions (i.e., SR Ca^{2+} release sites) may occur in highly ordered arrays, even though T-tubes twist and turn in a more complex way. The potential impact of the complex T-tubule topology on our results must be acknowledged, but the absence of detectable subsarcomeric Ca^{2+} gradients here is not likely due to geometric irregularities.

It is important to note that our recording system did resolve Ca^{2+} gradients in skeletal muscle fibers at equal sarcomere length. The absence of detectable Ca^{2+} gradients in the cardiac cells may be the result of a relatively slow AP-triggered SR Ca^{2+} release signal. This assumption is consistent with the longer time until first appearance of detectable Ca^{2+} release and the longer time to peak Ca^{2+} release (both parameters are $\sim$20 times slower in cardiac versus skeletal muscle cells). The apparently slower Ca^{2+} transient in cardiac cells is not likely due to differences in the release rates at the level of individual SR Ca^{2+} release channels. The permeation properties and activation kinetics of single cardiac and skeletal Ca^{2+} release channels are very similar (Györke et al., 1994). Furthermore, the rise time of local spontaneous Ca^{2+} sparks is nearly identical in cardiac and skeletal cells (Cheng et al., 1993; Tsugorka et al., 1995).

One explanation for the slower Ca^{2+} transient in cardiac muscle is the asynchronous recruitment of individual SR Ca^{2+} release units (or channels). Asynchronous recruitment of Ca^{2+} release units after the AP trigger signal would occur over ~100 ms (i.e., measured time to peak Ca^{2+} release). This relatively slow asynchronous recruitment effectively smears the local Ca^{2+} release profile because Ca^{2+} released at some sites would be diffusing away from others. The implication of this interpretation is that the highly synchronized AP-triggered Ca^{2+} release in skeletal muscle would ensure a fast maximum response. In contrast, the more asynchronous recruitment step in cardiac muscle would provide greater control because it represents a potential point for regulating the Ca^{2+} release process. Interestingly, the SR Ca^{2+} release in cardiac muscle is subject to regulation by a number of different pathways (i.e., β-adrenergic stimulation).

Numerical simulations of intracellular Ca^{2+} distribution were done to confirm our suspicion that the data could be explained by simple distributed diffusion arguments. The simulations show that subsarcomeric Ca^{2+} gradients are a consequence of the spatial arrangement of the Ca^{2+} release machinery in both skeletal and cardiac muscle. In other words, subsarcomeric Ca^{2+} gradients are a direct logical consequence of striated muscle morphology. The simulation, however, showed that the magnitude of the subsarcomeric Ca^{2+} gradient depends critically on the speed and synchrony of the local Ca^{2+} release function. Fast and highly synchronized Ca^{2+} release generates large subsarcomeric Ca^{2+} gradients. Slow and less synchronous Ca^{2+} release generates small subsarcomeric Ca^{2+} gradients. Our simulation also predicts that increasing Ca^{2+} indicator concentration and/or increasing Ca^{2+} buffer capacity of the cell increase the heterogeneity in Ca^{2+} distribution along the cell. These simulations were in good agreement with our experimental observations and with the modeling predictions of other authors (Cannell and Allen, 1984).

In summary, our data indicate that the spatial distribution of intracellular Ca^{2+} release sites, the speed/synchrony of the local Ca^{2+} release events, and diffusion are all key determinants of the spatiotemporal distribution of the local intracellular Ca^{2+} signals striated muscle cells.

We thank Dr. Carlo Caputo for helpful comments throughout this work. We also thank Dr. F. Herrera for loaning us the microscope objectives.

These studies were supported by CONICIT grant S1-95000493 (to PB), grant S1-95000587 (to AM), and National Institutes of Health grant HL57832 (to MF). MF is an Established Investigator of the American Heart Association.

REFERENCES

Armstrong, C., F. Bezanilla, and P. Horowitz. 1972. Twitches in the presence of ethylene glycol-bis(beta-aminoethyileter)-*N,N*′-tetraacetic acid. *Biochim. Biophys. Acta.* 267:605–608.

Beeler, G., and H. Reuter. 1970. The relation between membrane potential, membrane currents and activation of contraction in ventricular myocardial fibres. *J. Physiol. (Lond.).* 207:211–229.

Beuckelmann, D., and G. Wier. 1988. Mechanism of release of calcium from sarcoplasmic reticulum of guinea pig cardiac cells. *J. Physiol. (Lond.).* 405:233–255.

Cannell, M. B., and D. G. Allen. 1984. Model of calcium movements during activation in the sarcomere of frog skeletal muscle. *Biophys. J.* 45:913–925.

Caputo, C. 1968. The role of calcium in the processes of excitation and contraction in skeletal muscle. *J. Gen. Physiol.* 51(Suppl. 5):180S.

Caputo, C., P. Bolaños, and A. L. Escobar. 1999. Fast calcium removal during single twitches in amphibian skeletal muscle fibers. *J. Muscle Res. Cell Motil.* 20:555–567.

Cheng, H., W. J. Lederer, and M. B. Cannell. 1993. Calcium sparks: elementary events underlying excitation-contraction coupling in heart muscle. *Science.* 262:740–744.

Cleeman, L., W. Wang, and M. Morad. 1998. Two-dimensional confocal images of organization, density and gating of focal calcium release sites in rat cardiac myocytes. *Proc. Natl. Acad. Sci. USA.* 95:10984–10989.

Escobar, A., J. Monck, J. Fernández, and J. Vergara. 1994. Localization of the site of Ca^{2+} release at the level of a single sarcomere in skeletal muscle fibers. *Nature.* 367:739–741.

Fabiato, A. 1983. Calcium-induced release of calcium form the cardiac sarcoplasmic reticulum. *Am. J. Physiol.* 245:C1–C14.

Györke, S., P. Vélez, B. Suárez-Isla, and M. Fill. 1994. Activation of single cardiac and skeletal ryanodine receptor channels by flash photolysis of caged calcium. *Biophys. J.* 66:1879–1886.

Hille, B., and D. T. Campbell. 1976. An improved Vaseline-gap voltage-clamp for skeletal muscle fibers. *J. Gen. Physiol.* 67:265–293.

Isenberg, G., E. F. Etter, M. Wendt-Gallitelli, A. Schiefer, W. A. Carrington, R. A. Tuft, and F. S. Fay. 1996. Intrasarcomere calcium gradients in ventricular myocytes revealed by high speed digital imaging microscopy. *Proc. Natl. Acad. Sci. USA.* 93:5413–5418

Kovacs, L., E. Rios, and M. Schneider. 1979. Calcium transient and intramembrane charge movement in skeletal muscle fibers. *Nature.* 279:391–396.

Miledi, R., I. Parker, and G. Schalow. 1977. Measurement of calcium transients in frog skeletal muscle by the use of arsenazo III. *Proc. R. Soc. Lond. Biol.* 198:201–210.

Mitra, R., and M. Morad. 1985. A uniform enzymatic method for the dissociation of myocytes from hearts and stomachs of vertebrates. *Am. J. Physiol.* 249:H1056–H1060.

Monck, J., I. Robinson, A. Escobar, J. Vergara, and J. Fernández. 1994. Pulsed laser imaging of rapid Ca^{2+} gradients in excitable cells. *Biophys. J.* 67:505–514.

Näbauer, M., G. Callewaert, L. Cleemann, and M. Morad. 1989. Regulation of calcium release is gated by calcium current, not gating charge, in cardiac myocytes. *Science.* 244:800–803.

Pizarro, G., I. Csernoch, I. Uribe, M. Rodríguez, and E. Rios. 1991. The relationship between Qγ and calcium release from the sarcoplasmic reticulum in skeletal muscle. *J. Gen. Physiol.* 97:913–947.

Ríos, E., and G. Pizarro. 1991. Voltage sensor of excitation-contraction coupling in skeletal muscle. *Physiol. Rev.* 71:849–908.

Sandow, A. 1965. Excitation-contraction coupling in skeletal muscle. *Pharmacol. Rev.* 17:265–320.

Schneider, M., and W. Chandler. 1973. Voltage dependence charge movement in skeletal muscle: a possible step in excitation-contraction coupling. *Nature.* 242:244–246.

Shirokova, N., J. García, G. Pizarro, and E. Ríos. 1996. Ca^{2+} release from the sarcoplasmic reticulum compared in amphibian and mammalian skeletal muscle. *J. Gen. Physiol.* 107:1–18.

Soeller, C., and M. B. Cannell. 1999. Examination of the transverse tubular system in living cardiac rat myocytes by 2-photon microscopy and digital image processing techniques. *Circ. Res.* 84:266–275.

Tsugorka, A., E. Rios, and L. Blatter. 1995. Imaging of elementary events of calcium release in skeletal muscle cells. *Science.* 269:1723–1726.

Vergara, J., F. Bezanilla, and B. M. Salzberg. 1978. Nile blue fluorescence signals from cut single muscle fibers under voltage or current clamp conditions. *J. Gen. Physiol.* 72:775–800.